

Bases for C_0 - P_1 divergence-free elements and for C_1 - P_2 finite elements on union jack grids

Shangyou Zhang*

Dedicated to the memory of Gene H. Golub

Abstract

It is a challenge to find point wise (including inter-element boundary) divergence-free finite element bases. By identifying functions in the kernel of the divergence operator, we discover a local basis for the full divergence-free space of the C_0 - P_1 finite element, on the union jack grid. The optimal order of approximation is shown for the P_1 divergence-free finite elements on union jack grids, and numerical tests are provided, solving stationary Stokes equations.

We further compute the anti-derivative of such divergence-free basis functions to construct a C_1 - P_2 basis for the continuously-differentiable, piecewise quadratic polynomial space on union jack grids. The full approximation property of the C_1 - P_2 space is established. The C_1 - P_2 basis is applied to the biharmonic equation. The optimal order of convergence is proved. Numerical tests are presented to support the analysis.

Keywords. finite element, Stokes equations, divergence-free element, Powell-Sabin triangulation, union jack grid, biharmonic equation, continuously differentiable finite element, spline.

AMS subject classifications (2000). 65M60, 65N30, 76M10, 76D07.

1 Introduction

A main difficulty in computational fluid dynamics is to treat mass conservation, i.e., to preserve the incompressibility (divergence-free) condition. Many techniques and constructions were developed in finite element methods for approximating the incompressible Stokes or Navier-Stokes flows, in the past thirty years, cf. [19, 5]. Nevertheless, it is generally believed, for example, stated in [5], that it is difficult to construct low order divergence-free mixed elements, if not impossible. A fundamental study on the divergence-free element was done by Scott and Vogelius in 1983 ([20, 21]) that the method is stable and of optimal order for the C_0 - $P_k/C_{-1} - P_{k-1}$ element, $k \geq 4$, provided that the 2D triangular grids have no nearly-singular vertex. That is, the divergence-free C_0 - P_k piecewise polynomial space has an optimal order approximation for all $k \geq 4$. In [20], it is shown that the divergence-free element is not stable for $k \leq 3$ for general triangular grids. But on special grids, some low order divergence-free elements were discovered, cf. [2, 18, 25, 27].

*Department of Mathematical Sciences, University of Delaware, DE 19716. szhang@udel.edu.

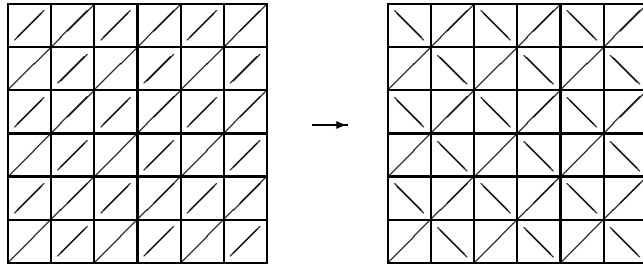


Figure 1: A criss grid and a union jack grid (flip one edge on every other square).

The P_1 - P_0 element on uniform grids (see the first grid in Figure 1) is used in textbooks as a counter-example showing the necessity in matching the pair of finite element spaces. The discrete solutions for the velocity would approach zero instead of the true solution, on uniform criss grids shown in Figure 1, forced by the divergence-free condition, known as locking phenomenon, cf. [5, 27]. However, we discovered that this problem has a simple cure. We can alter one edge on every other square of a criss grid to get a union jack grid, see the second grid in Figure 1. The union jack grid is a kind of Powell-Sabin triangulations (cf. Figure 2), based on a quadrilateral grid, instead of a triangular grid, cf. [17, 27]. It is done by connecting the bary-center of each quadrilateral to its four vertices, and to the centers of neighboring quadrilaterals, see Figure 2. That is, each quadrilateral is subdivided into eight triangles. In this manuscript, we will find the kernel of the divergence operator and construct a local basis for the kernel space, i.e., a divergence-free subspace of the C_0 - P_1 element space on the union jack grids. We will show the optimal order of this lowest order P_1 finite element, which is also divergence-free point wise. To preserve incompressibility better or in higher orders, discontinuous Galerkin and non-conforming elements were designed and studied recently, cf. [1, 8, 15]. These elements are divergence-free locally only, but not on inter-element boundary.

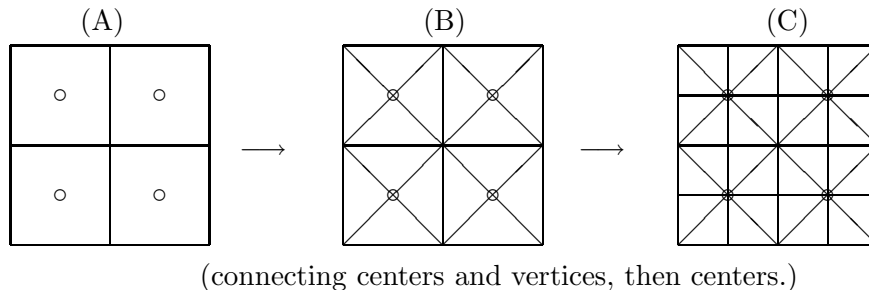


Figure 2: A quadrilateral-based Powell-Sabin grid.

After we discover a local basis for the P_1 divergence-free space, following the approach in [18, 26], we find the C_1 - P_2 potential functions for these C_0 - P_1 basis functions. This generates a local basis for C_1 - P_2 finite element space. This C_1 - P_2 basis is somewhat new. It is a 45-degree rotation of the Zwart basis [29], discovered in 1973. The dimension and application of C_1 - P_2 functions, known as B-spline functions, on union jack grids were developed in [9, 10, 24, 11], based on the Bernstein-Bézier representation. Nevertheless, in the finite element method, a locally supported basis is necessary for computation. It is pointed out by Chui and Wang [6, 7] that the Zwart basis functions are not linearly independent on the whole plane R^2 . However, the Zwart basis (and its 45-degree rotation cousin here) does form a basis on finite domains with both C_0 and C_1 boundary conditions. We prove it by an averaging interpolation operator,

which is constructed by a dual basis for the C_1-P_2 space under $L^2(\Omega)$ inner-product. We note that a different interpolation operator based on certain nodal values for C_0-P_2 splines was proposed recently by Sorokina and Zeilfelder in [24]. Our interpolation operator is based on the integral values of functions against the dual basis functions. With this interpolation operator, the optimal order approximation for the C_1-P_2 space on the union jack grid is established. In fact, from the convergence of C_1-P_2 element for the biharmonic equation, we deduce the convergence of C_0-P_1 divergence-free element for the Stokes equations.

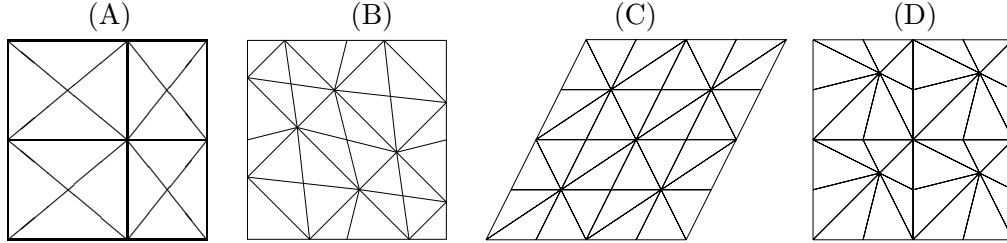


Figure 3: A rectangular criss-cross grid, three perturbed union jack grids.

As pointed out above, the C_0-P_1 divergence free space does not provide any approximation on the criss grid shown in Figure 1. The element also does not work on general union jack grids, for example, which are based on general quadrilaterals instead of squares, cf. Figure 3. In this case, we need increase the polynomial degree from 1 to 2, as studied by Arnold and Qin in [2]. For perturbed union jack grids shown as in Figure 3(D), the polynomial degree could be even higher. However, Scott and Vogelius proved it that C_0-P_k divergence-free element works on general quasiuniform grids for $k \geq 4$. On the other hand, the analysis provided in this manuscript can be extended to cover a kind of slightly perturbed union jack grids, which are refined from rectangular/parallelogram grids except at the boundary, as shown in Figure 3(B) and Figure 3(C). This is confirmed somewhat by our numerical tests. We note that the grid in Figure 3(B) is a rotation of a rectangular criss-cross grid, like the one shown in 3(A). The Zwart basis has been generalized to non square criss-cross grids, shown in 3(A), by Chui and Wang [6].

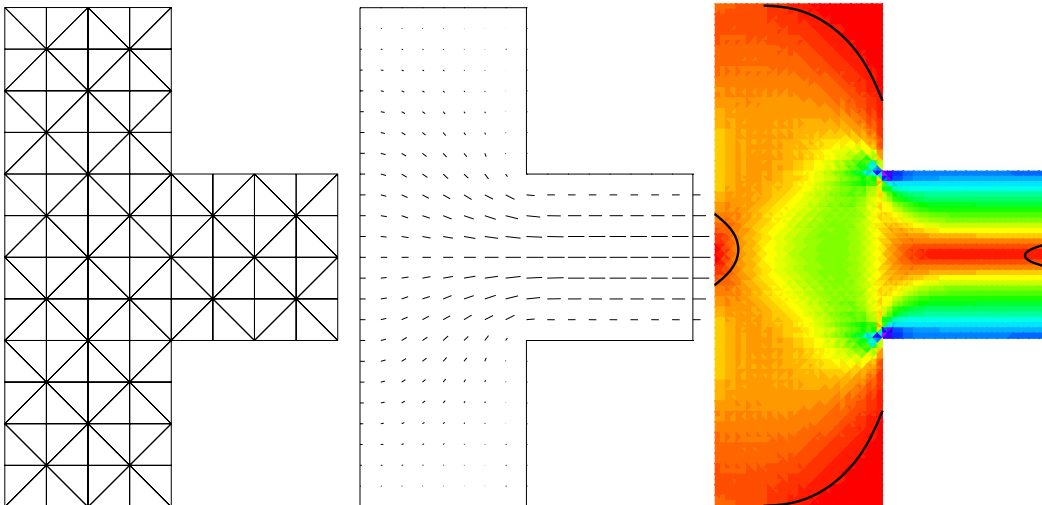


Figure 4: A union jack grid, computed velocity field and strain field.

It is well known that the 2D Stokes equations can be converted to a biharmonic equation for the stream function, cf. [21, 19]. Consequently, the C_0 - P_1 velocity is the curl of the C_1 - P_2 stream function on the same grid. In this direction, Lai and coworkers applied the C_1 -splines to solve Stokes and Navier-Stokes in 2D and 3D [13, 3, 14]. However, we do not have local basis functions for these splines. It is required in the finite element method. It seems there is only one work so far, identifying a local basis for the full C_1 - P_k space ($k \geq 5$) on a general grid, by Morgan and Scott [16] in 1975. Of course, there are works either on constructing a subspace of C_1 polynomials such as [28], or the full C_1 space but on special grids such as [29, 26] and this research.

Theoretically, the P_1 divergence-free velocity from the mixed element equations (2.7) is the same as the P_1 divergence-free projection in (2.15), and the same as the curl of the C_1 - P_2 stream function from the biharmonic problem (4.11). Computationally, the three methods are different. Probably the first method is the best, though it has an indefinite system with much more unknowns. We refer readers to Section 5. In particular, the coding work is minimal for the first method, by the mixed element equations (2.7). A big difference is in treating inhomogeneous boundary conditions, for example, shown in Figure 4, see Section 5 for more information. It is very difficult to produce appropriate boundary conditions for the projection problem (2.15) and for the C_1 - P_2 biharmonic problem (4.11).

Though we constructed the divergence-free space and showed the convergence of divergence-free C_0 - P_1 finite element solutions, such a pair of P_1 - P_0 finite elements does not satisfy the inf-sup stability condition, cf. [19]. In fact, the finite-element pressure computed on union jack grids does not converge to the true solution at all. But it does converge on the 45-degree rotated grids, the criss-cross grids, shown in Figure 2(B). Readers are referred to the comments in the section of numerical test below. Further analysis is needed on the problem.

The rest of the paper is organized as follows. In Section 2, we define the P_1 - P_0 mixed element and find all spurious pressure modes. Then we are able to construct a divergence-free P_1 basis. In Section 3, we define a C_1 - P_2 finite element, induced by the P_1 divergence-free functions. In Section 4, we prove the convergence for both P_1 divergence-free elements and C_1 - P_2 elements. In Section 5, we apply the C_1 - P_2 element and the P_1 divergence-free element for solving the biharmonic equation and the Stokes equations, respectively, confirming the analysis.

2 The P_1 - P_0 divergence-free element

We solve a model stationary Stokes problem: Find the velocity function \mathbf{u} and the pressure p on a square domain $\Omega = (0, 1)^2$, such that

$$\begin{aligned} -\Delta \mathbf{u} + \nabla p &= \mathbf{f} && \text{in } \Omega, \\ \operatorname{div} \mathbf{u} &= 0 && \text{in } \Omega, \\ \mathbf{u} &= \mathbf{0} && \text{on } \partial\Omega. \end{aligned} \tag{2.1}$$

The variational form for (2.1) is: Find $\mathbf{u} \in H_0^1(\Omega)^2$ and $p \in L_0^2(\Omega) := L^2(\Omega)/C = \{p \in L^2 \mid \int_{\Omega} p = 0\}$ such that

$$\begin{aligned} a(\mathbf{u}, \mathbf{v}) + b(\mathbf{v}, p) &= (\mathbf{f}, \mathbf{v}) \quad \forall \mathbf{v} \in H_0^1(\Omega)^2, \\ b(\mathbf{u}, q) &= 0 \quad \forall q \in L_0^2(\Omega). \end{aligned} \tag{2.2}$$

Here $H_0^1(\Omega)^2$ is the subspace of the Sobolev space $H^1(\Omega)^2$ (cf. [5, 19]) with zero boundary trace, $a(\mathbf{u}, \mathbf{v}) = (\nabla \mathbf{u}, \nabla \mathbf{v})$, $b(\mathbf{v}, p) = -(\operatorname{div} \mathbf{u}, p)$ and (\cdot, \cdot) is the L^2 inner product.

Let Ω be subdivided into n^2 uniform rectangles,

$$\bar{\Omega}_h = \{Q \mid Q = [x_i, x_i + h] \times [y_j, y_j + h], 0 \leq i, j < n\}, \quad (2.3)$$

where $h = 1/n$. Connecting the center of each square with its vertices and mid-edge points (see Figure 2), we define the resulting Powell-Sabin triangulation by

$$\Omega_h = \{K_i \mid \cup K_i = Q \quad \forall Q \in \bar{\Omega}_h\}. \quad (2.4)$$

The P_1 - P_0 divergence-free element spaces are

$$\mathbf{V}_h = \{\mathbf{u}_h \in C(\Omega)^2 \mid \mathbf{u}_h|_K \in P_1(K)^2 \quad \forall K \in \Omega_h, \text{ and } \mathbf{u}_h|_{\partial\Omega} = 0\}, \quad (2.5)$$

$$P_h = \{\text{div } \mathbf{u}_h \mid \mathbf{u}_h \in \mathbf{V}_h\}. \quad (2.6)$$

Since $\int_{\Omega} p_h = \int_{\Omega} \text{div } \mathbf{u}_h = \int_{\partial\Omega} \mathbf{u}_h \cdot \mathbf{n} = 0$ for any $p_h \in P_h$, we conclude that $P_h \subset L_0^2(\Omega)$. The resulting system of finite element equations for (2.2) is: Find $\mathbf{u}_h \in \mathbf{V}_h$ and $p_h \in P_h$ such that

$$\begin{aligned} a(\mathbf{u}_h, \mathbf{v}_h) + b(\mathbf{v}_h, p_h) &= (\mathbf{f}, \mathbf{v}_h) \quad \forall \mathbf{v}_h \in \mathbf{V}_h, \\ b(\mathbf{u}_h, q_h) &= 0 \quad \forall q_h \in P_h. \end{aligned} \quad (2.7)$$

By the second equation in (2.7) and the definition of P_h in (2.6), we conclude that

$$b(\mathbf{u}_h, q) = b(\mathbf{u}_h, -\text{div } \mathbf{u}_h) = \|\text{div } \mathbf{u}_h\|_{L^2(\Omega)^2}^2 = 0.$$

Thus $\text{div } \mathbf{u}_h$ is also point wise 0 everywhere. In this case, we call the mixed finite element a divergence-free element. For the divergence-free element, the equation (2.7) always has a unique solution, cf. [27]. In addition, it is trivial to show ([19, 5, 4, 27]) that \mathbf{u}_h is the unique $a(\cdot, \cdot)$ orthogonal projection from the divergence-free space $\mathbf{Z} = H_0^1(\Omega)^2 \cap \{\text{div } \mathbf{v} = 0\}$ to its subspace

$$\mathbf{Z}_h = \mathbf{V}_h \cap \{\text{div } \mathbf{v} = 0 \mid \mathbf{v} \in H_0^1(\Omega)^2\}.$$

We note that by (2.6), P_h is a subspace of piecewise constants. As singular vertices are present (see [20, 21]), P_h is a proper subset of the piecewise constants space in L_0^2 . We identify some spurious modes in P_h next.

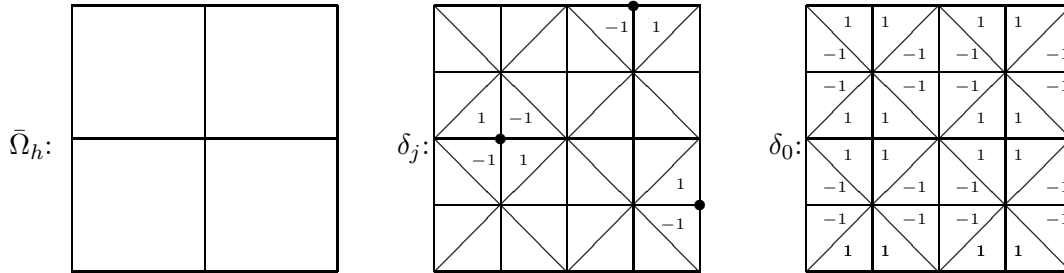


Figure 5: A quadrilateral grid, and spurious pressure modes on the union jack grid.

For each mid-edge point $\mathbf{x}_k = (x_i, y_j)$ of squares in $\bar{\Omega}_h$, see (2.3) and Figure 5, we define one singular vertex pressure mode:

$$\delta_k(x, y) = \begin{cases} -1, & (x, y) = (x_i^-, y_j^-), \\ -1, & (x, y) = (x_i^+, y_j^+), \\ 1, & (x, y) = (x_i^+, y_j^-), \\ 1, & (x, y) = (x_i^-, y_j^+), \\ 0, & (x, y) \in K \text{ \& } (x_i^\pm, y_j^\pm) \notin K, \end{cases} \quad (2.8)$$

$1 \leq k \leq 2n(n+1)$. Here $\delta_k(x, y)$ is extended to be piecewise constant on each $K \in \Omega_h$. In addition to a global constant (which is filtered out in L_0^2 space), there is one global pressure spurious mode (see Figure 5):

$$\delta_0(x, y) = \begin{cases} 1, & (x, y) \in K \text{ which has a horizontal mid-edge point vertex,} \\ -1, & (x, y) \in K \text{ which has a vertical mid-edge point vertex.} \end{cases} \quad (2.9)$$

Lemma 2.1 *Let P_h be defined in (2.6).*

$$P_h \subset S_h := \{q_h \mid q_h|_K \in P_0 \ \forall K \in \Omega_h, \quad (q_h, \delta_k) = 0, \ -1 \leq \delta_k \leq 2n(n+1)\}, \quad (2.10)$$

where $\delta_{-1} \equiv 1$ on Ω , and δ_k are defined in (2.8) and (2.9).

Proof. Let $q_h \in P_h$. q_h is a piecewise constant function and it is equal to $\text{div } \mathbf{w}_h$ for some $\mathbf{w}_h \in \mathbf{V}_h$ by the definition (2.6). Let $\{\phi_i\}$ and $\{\psi_j\}$ be the P_1 nodal basis functions at all internal, mid-edge points \mathbf{x}_i and at vertices \mathbf{y}_i of quadrilaterals in $\bar{\Omega}_h$, respectively, i.e.,

$$\begin{aligned} \phi_i(\mathbf{x}_i) &= 1, & \phi_i(\mathbf{x}_j) &= 0, \quad j \neq i, & \phi_i(\mathbf{y}_j) &= 0; \\ \psi_i(\mathbf{x}_j) &= 0, & \psi_i(\mathbf{y}_j) &= 0, \quad j \neq i, & \psi_i(\mathbf{y}_i) &= 1. \end{aligned}$$

Avoiding too many notations, we plot the derivatives of these basis functions in Figure 6.

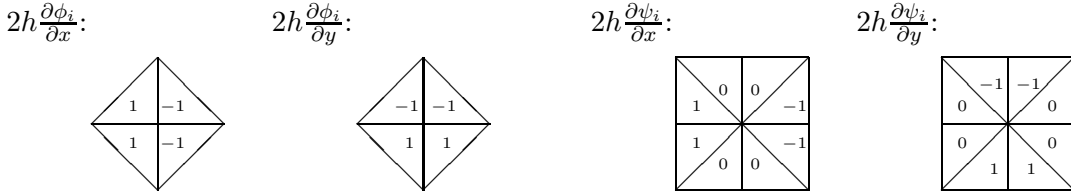


Figure 6: Partial derivatives (scaled by $2h$) at \mathbf{x}_i and \mathbf{y}_j .

By Figures 5 and 6, we find that

$$\begin{aligned} ((\phi_i)_x, \delta_k) &= ((\phi_i)_y, \delta_k) = ((\psi_j)_x, \delta_k) = ((\psi_j)_y, \delta_k) = 0, \\ &\text{for all } 1 \leq i \leq 2n(n-1), \ 1 \leq j \leq n^2 + (n-1)^2, \ -1 \leq k \leq 2n(n+1). \end{aligned}$$

Expanding \mathbf{w}_h under the nodal basis, we get

$$\begin{aligned} (q_h, \delta_k) &= (\text{div } \mathbf{w}_h, \delta_k) = (\text{div } \sum_i \begin{pmatrix} u_{i1} \\ u_{i2} \end{pmatrix} \phi_i + \text{div } \sum_j \begin{pmatrix} v_{j1} \\ v_{j2} \end{pmatrix} \psi_j, \delta_k) \\ &= \sum_i u_{i1}((\phi_i)_x, \delta_k) + \sum_i u_{i2}((\phi_i)_y, \delta_k) + \\ &\quad \sum_j v_{j1}((\psi_j)_x, \delta_k) + \sum_h b_{j2}((\psi_j)_y, \delta_k) = 0. \end{aligned}$$

Therefore $q_h \in S_h$. ■

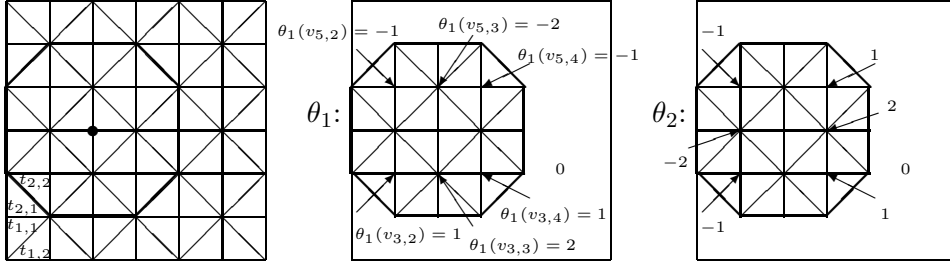


Figure 7: Nodal values (0 for rest) of a divergence-free basis function, $\vec{\theta}_{4,3}$.

After we find enough functions in \mathbf{Z}_h , the kernel of div operator on \mathbf{V}_h , we will conclude that $P_h = S_h$. Let $\theta_1(x, y), \theta_2(x, y)$ be C_0 - P_1 functions defined by Figure 7, supported on 9 rotated squares, i.e., diamonds. Let us number vertices and triangles in Ω_h as follows: $v_{i,j}$ denotes the j -th vertex on i -th row; $t_{i,j}$ denotes the j -th triangle counting from left on i -th row of triangles. By these notations, we have, cf. Figure 7,

$$\theta_1(\mathbf{x}) = \begin{cases} 1 & \mathbf{x} = v_{3,2}, v_{3,4}, \\ 2 & \mathbf{x} = v_{3,3}, \\ -1 & \mathbf{x} = v_{5,2}, v_{5,4}, \\ -2 & \mathbf{x} = v_{5,3}, \\ 0 & \mathbf{x} = \text{rest } v_{i,j}; \end{cases} \quad (2.11)$$

$$\theta_2(\mathbf{x}) = \begin{cases} 1 & \mathbf{x} = v_{3,4}, v_{5,4}, \\ 2 & \mathbf{x} = v_{4,4}, \\ -1 & \mathbf{x} = v_{3,2}, v_{5,2}, \\ -2 & \mathbf{x} = v_{4,2}, \\ 0 & \mathbf{x} = \text{rest } v_{i,j}. \end{cases} \quad (2.12)$$

In (2.11) and (2.12), θ_i is defined by its nodal values at vertices. $\theta_1(x, y)$ and $\theta_2(x, y)$ are piecewise linear functions, determined by their nodal values specified in (2.11) and (2.12), at vertices of triangulation Ω_h . Side by side, we plot the two components of one $\vec{\theta} = \langle \theta_1, \theta_2 \rangle$ in Figure 8.

Lemma 2.2 *Let $\vec{\theta}_{i,j}$ be defined in (2.11), (2.12) and Figure 7. There are $2(n-1)(n-2)$ divergence-free, linearly independent functions in \mathbf{V}_h , on the union jack grid Ω_h of $8n^2$ triangles, i.e., (cf. Figure 9)*

$$\vec{\theta}_{2j,2i-1}, \vec{\theta}_{2i-1,2j} \in \mathbf{Z}_h, \quad 1 < i < n-1, \quad 1 < j < n. \quad (2.13)$$

Proof. It is straightforward to verify $\text{div } \vec{\theta}_{2j,2i-1} = 0$, by adding the two partial derivatives of two components of $\vec{\theta}_{2j,2i-1}$, shown in Figure 10. If these $2(n-1)(n-2)$ functions are linearly dependent, we then have a nonzero linear combination to get 0,

$$\sum a_{i,j} \vec{\theta}_{i,j} = 0.$$

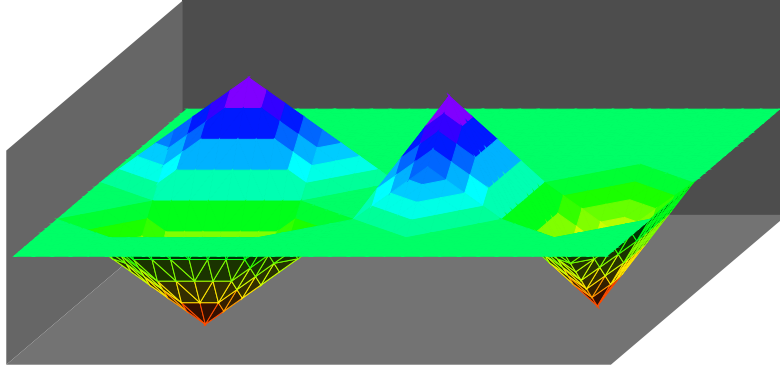


Figure 8: The two components (side by side) of one divergence free basis function.

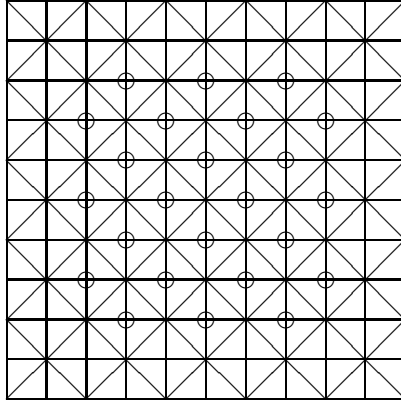


Figure 9: The centers of divergence-free functions, $\vec{\theta}_{i,j}$.

Among those nonzero coefficients $\{a_{k,l}\}$, we pick up one which is associated to a $\vec{\theta}_{k_0,l_0}$ closest to the boundary (pick up anyone if more than one.) We get then

$$\vec{\theta}_{k_0,l_0} = \sum_{(i,j) \neq (k,l)} b_{i,j} \vec{\theta}_{i,j}.$$

But this is a contradiction, because for everyone $\vec{\theta}_{k_0,l_0}$ on the outside ring, see Figure 9, there are two triangles on which $\vec{\theta}_{i_0,j_0} \neq \mathbf{0}$ while all rest $\vec{\theta}_{i,j} = \mathbf{0}$.

■

Theorem 2.1 Let $\vec{\theta}_{i,j}$ be defined in (2.11), (2.12) and Figure 7. Then $\dim \mathbf{Z}_h = 2(n-1)(n-2)$, and

$$\mathbf{Z}_h = \text{span}\{\vec{\theta}_{2j,2i-1}, \vec{\theta}_{2i-1,2j} \mid 1 < i < n-1, 1 < j < n\}. \quad (2.14)$$

Proof. Since $\text{div} : \mathbf{V}_h \rightarrow P_h$ and $\text{kernel}(\text{div}) = \mathbf{Z}_h$, we have

$$\dim \mathbf{Z}_h = \dim \mathbf{V}_h - \dim P_h \leq \dim \mathbf{V}_h - \dim S_h,$$

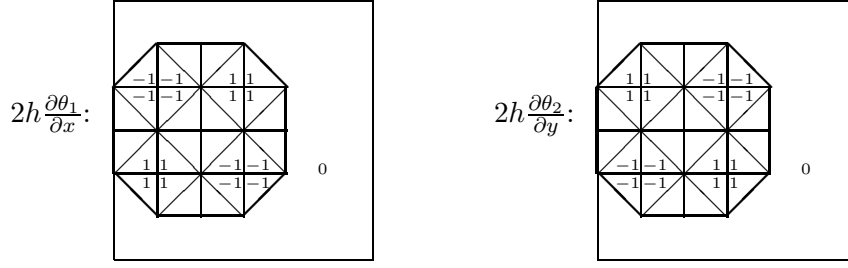


Figure 10: Two partial derivatives of two components of $\vec{\theta}_{4,3}$, note that $\text{div } \vec{\theta}_{4,3} = 0$.

where we applied (2.10) in the last step. As we have $8n^2$ triangles in Ω_h , by (2.10), we get

$$\dim S_h = 8n^2 - (2n(n+1) + 2) = 6n^2 - 2n - 2.$$

By counting interior vertices, we get that

$$\dim \mathbf{V}_h = 2[(n-1)^2 + n^2 + 2n(n-1)] = 8n^2 - 8n + 2.$$

Thus

$$\dim \mathbf{Z}_h \leq (8n^2 - 8n + 2) - (6n^2 - 2n - 2) = 2n^2 - 6n + 4 = 2(n-2)(n-1).$$

As we found $2(n-2)(n-1)$ linearly independent vectors in \mathbf{Z}_h , by (2.13), we conclude $\dim Z_h = 2(n-2)(n-1)$. The theorem is proved. \blacksquare

Once we have a local basis for the divergence-free space \mathbf{Z}_h , the mixed finite problem (2.7) can be reduced to the following positive definite problem: Find $\mathbf{u}_h \in \mathbf{Z}_h$ such that

$$a(\mathbf{u}_h, \mathbf{v}_h) = (\mathbf{f}, \mathbf{v}_h) \quad \forall \mathbf{v}_h \in \mathbf{Z}_h. \quad (2.15)$$

We will prove the optimal-order approximation of \mathbf{Z}_h after we analyze the “potential space” of C_1 - P_2 functions.

3 The C_1 - P_2 space on union jack grids

We integrate the first component of each basis function, defined in (2.11), of P_1 -divergence free finite element space against y to obtain a local basis for the space of differentiable piecewise quadratic polynomials. Such a C_1 - P_2 basis function is plotted in Figure 11. The integration is done triangle by triangle, cf. Figures 7, 12 and 13 below. By Figure 7 and (2.11), we first recover the piecewise linear polynomial definition for θ_1 , shown in Figure 12, where we plot only one fourth support of θ_1 as the rest can be easily seen by symmetry. We present the C_1 - P_2 basis functions constructed this way next.

We first define three piecewise C_1 - P_2 polynomials on the unit square at the origin, see

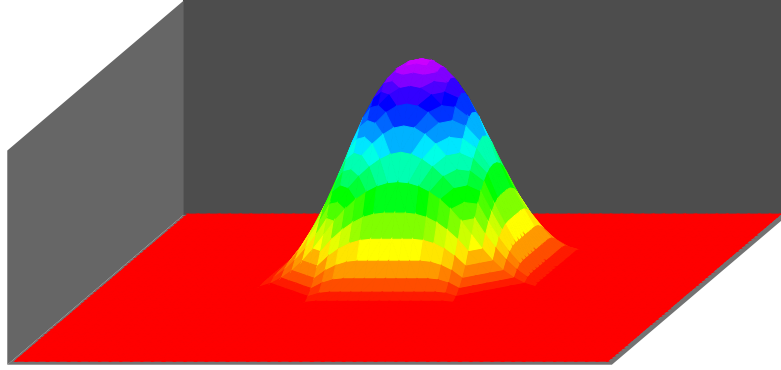


Figure 11: A C_1 - P_2 local basis function on the union jack grid.

Figure 12.

$$\tau_1(x, y) = \begin{cases} 0 & x + y \leq 1, (x, y) \in (0, 1)^2, \\ \frac{(x+y-1)^2}{2} & x + y \geq 1, (x, y) \in (0, 1)^2; \end{cases} \quad (3.1)$$

$$\tau_2(x, y) = \begin{cases} y^2 & x - y \geq 0, (x, y) \in (0, 1)^2, \\ \frac{y^2+2xy-x^2}{2} & x - y \leq 0, (x, y) \in (0, 1)^2; \end{cases} \quad (3.2)$$

$$\tau_3(x, y) = \begin{cases} \frac{1+2(x+y)-(x-y)^2}{2} & x + y \leq 1, (x, y) \in (0, 1)^2, \\ \frac{2x+2y-x^2-y^2}{2} & x + y \geq 1, (x, y) \in (0, 1)^2; \end{cases} \quad (3.3)$$

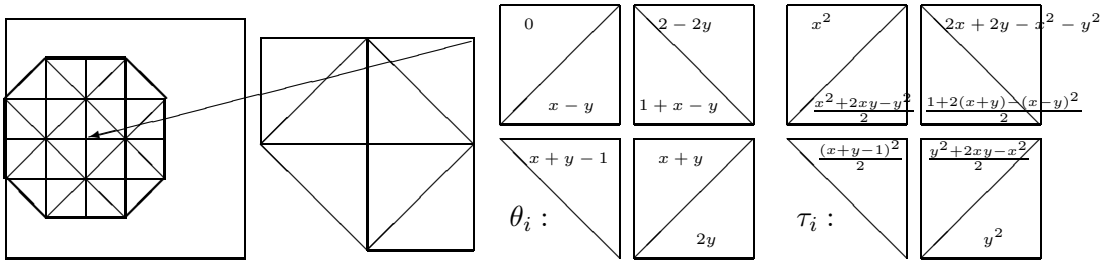


Figure 12: The definition of $\vec{\theta}_{4,3}$ on a quarter of its support, and that of $\tau_{4,3}$.

We now define basis functions for C_1 - P_2 finite element spaces. As in the last section, we

use $\{v_{i,j} = (x_i, y_j)\}$ to denote vertices of union jack grid Ω_h .

$$\tau_{i,j}(x, y) = \begin{cases} \tau_3\left(\frac{2(x-x_{i-1})}{h}, \frac{2(y-y_{j-1})}{h}\right) & (x, y) \in (x_{i-1}, x_i) \times (y_{j-1}, y_j), \\ \tau_3\left(\frac{2(x_{i+1}-x)}{h}, \frac{2(y-y_{j-1})}{h}\right) & (x, y) \in (x_i, x_{i+1}) \times (y_{j-1}, y_j), \\ \tau_3\left(\frac{2(x-x_{i-1})}{h}, \frac{2(y_{j+1}y-y)}{h}\right) & (x, y) \in (x_{i-1}, x_i) \times (y_j, y_{j+1}), \\ \tau_3\left(\frac{2(x_{i+1}-x)}{h}, \frac{2(y_{j+1}-y)}{h}\right) & (x, y) \in (x_i, x_{i+1}) \times (y_j, y_{j+1}), \\ \tau_2\left(\frac{2(x-x_{i-1})}{h}, \frac{2(y-y_{j-2})}{h}\right) & (x, y) \in (x_{i-1}, x_i) \times (y_{j-2}, y_{j-1}), \\ \tau_2\left(\frac{2(x_{i+1}-x)}{h}, \frac{2(y-y_{j-2})}{h}\right) & (x, y) \in (x_i, x_{i+1}) \times (y_{j-2}, y_{j-1}), \\ \tau_2\left(\frac{2(y_j-y)}{h}, \frac{2(x_{i+2}-x)}{h}\right) & (x, y) \in (x_{i+1}, x_{i+2}) \times (y_{j-1}, y_j), \\ \tau_2\left(\frac{2(y-y_j)}{h}, \frac{2(x_{i+2}-x)}{h}\right) & (x, y) \in (x_{i+1}, x_{i+2}) \times (y_j, y_{j+1}), \\ \tau_2\left(\frac{2(x-x_{i-1})}{h}, \frac{2(y_{j+2}-y)}{h}\right) & (x, y) \in (x_{i-1}, x_i) \times (y_{j+1}, y_{j+2}), \\ \tau_2\left(\frac{2(x_{i+1}-x)}{h}, \frac{2(y_{j+2}-y)}{h}\right) & (x, y) \in (x_i, x_{i+1}) \times (y_{j+1}, y_{j+2}), \\ \tau_2\left(\frac{2(y_j-y)}{h}, \frac{2(x-x_{i-2})}{h}\right) & (x, y) \in (x_{i-2}, x_{i-1}) \times (y_{j-1}, y_j), \\ \tau_2\left(\frac{2(y-y_j)}{h}, \frac{2(x-x_{i-2})}{h}\right) & (x, y) \in (x_{i-2}, x_{i-1}) \times (y_j, y_{j+1}), \\ \tau_1\left(\frac{2(x-x_{i-2})}{h}, \frac{2(y-y_{j-2})}{h}\right) & (x, y) \in (x_{i-2}, x_{i-1}) \times (y_{j-2}, y_{j-1}), \\ \tau_1\left(\frac{2(x_{i+2}-x)}{h}, \frac{2(y-y_{j-2})}{h}\right) & (x, y) \in (x_{i+1}, x_{i+2}) \times (y_{j-2}, y_{j-1}), \\ \tau_1\left(\frac{2(x_{i+2}-x)}{h}, \frac{2(y_{j+2}-y)}{h}\right) & (x, y) \in (x_{i+1}, x_{i+2}) \times (y_{j+1}, y_{j+2}), \\ \tau_1\left(\frac{2(x-x_{i-2})}{h}, \frac{2(y_{j+2}-y)}{h}\right) & (x, y) \in (x_{i-2}, x_{i-1}) \times (y_{j+1}, y_{j+2}), \\ 0 & \text{on rest squares.} \end{cases} \quad (3.4)$$

We note that we do not need to switch x and y on some squares in (3.4) as both τ_1 and τ_3 are symmetric functions.

Lemma 3.1 *The local basis functions,*

$$\tau_{2i-1,2j} \quad \text{and} \quad \tau_{2j,2i-1}, \quad 1 < i < (n-1), \quad 1 < j < n,$$

are continuously differentiable, piecewise quadratic polynomials on the union jack grid Ω_h .

Proof. By our construction, we have, point wise,

$$\begin{pmatrix} \frac{\partial}{\partial y} \tau_{2i-1,2j} \\ -\frac{\partial}{\partial x} \tau_{2i-1,2j} \end{pmatrix} = \vec{\theta}_{2i-1,2j} \in \mathbf{V}_h \subset C(\Omega)^2. \quad \blacksquare$$

Though we give the piecewise definition for the quadratic polynomials $\tau_{i,j}$ on each square, one may not need it in practice. Instead, computationally, it is often to represent these C_1 - P_2 basis functions by the linear combinations of the standard Lagrange nodal basis. For this purpose, we list the nodal values of $\frac{1}{2}\tau_{i,j}$ at all P_2 Lagrange nodes in Figure 13. So $\tau_{i,j}$ is a linear combination of 45 Lagrange nodal basis functions, by Figure 13.

To conclude this section, we introduce a model biharmonic equation and its finite element solution. Let us consider the clamped plate bending problem, finding the solution of the following biharmonic equation with homogeneous boundary conditions,

$$\begin{cases} \Delta^2 w = g, & \text{in } \Omega = (0, 1)^2, \\ w = 0 & \text{on } \partial\Omega, \\ \frac{\partial w}{\partial \mathbf{n}} = 0 & \text{on } \partial\Omega. \end{cases} \quad (3.5)$$

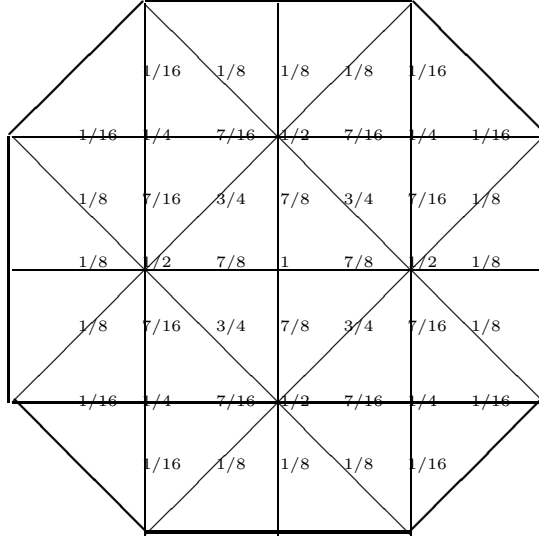


Figure 13: The values of $\frac{1}{2}\tau_{i,j}$, a C_1 - P_2 basis function, at Lagrange nodes.

Via integration by parts, we introduce a variational problem for (3.5): finding $w \in H_0^2(\Omega)$ such that

$$\int_{\Omega} \Delta w \Delta v = \int_{\Omega} g v \quad \forall v \in H_0^2(\Omega).$$

Let W_h be defined by the linear span of the above C_1 - P_2 basis functions on Ω_h :

$$W_h = \text{span}\{\tau_{2i-1,2j}, \tau_{2j,2i-1}, 1 < i < (n-1), 1 < j < n\}. \quad (3.6)$$

We will prove that the above span is unique, i.e., $\{\tau_{i,j}\}$ are truly linear independent, in Lemma (4.2). The finite element solution w_h is defined by

$$(\Delta w_h, \Delta v_h) = (g, v_h) \quad \forall v_h \in W_h. \quad (3.7)$$

4 Convergence

We will show the approximation property of the C_1 - P_2 space W_h first. Based on this, we would prove the optimal order of approximation of C_0 - P_1 divergence-free space \mathbf{Z}_h . It seems difficult to show the approximation property of \mathbf{Z}_h without using the inf-sup condition (see [5, 19]). As a matter of fact, we are not able to establish the inf-sup condition with a constant independent of grid side h , for the current P_1/P_0 divergence-free element.

Lemma 4.1 *Let $v(x, y) \in P_2(D_{i,j})$, where, see Figure 14,*

$$D_{i,j} = \{(x, y) \mid -\frac{h}{2} \leq x + y - x_i - y_j \leq \frac{2}{h}, -\frac{h}{2} \leq x - y - x_i + y_j \leq \frac{2}{h}\}.$$

Then, letting

$$M = \{(0, 0), (0, \pm 2), (\pm 2, 0), (\pm 1, \pm 1)\} \quad (4.1)$$

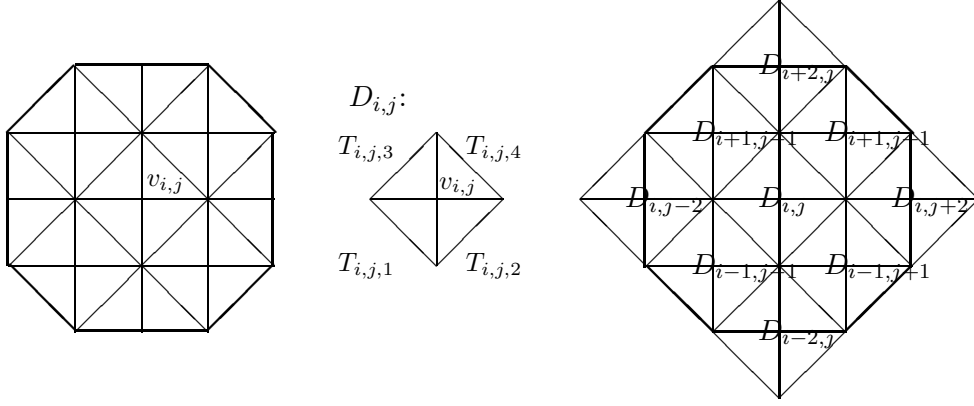


Figure 14: Subdivide the support of $\tau_{i,j}$ into 9 parts, $D_{i+k,j+l}$.

be an index set (see Figure 14),

$$v(x, y) = \sum_{(k,l) \in M} v_{k,l} \tau_{i+k,j+l}(x, y) \quad \forall (x, y) \in D_{i,j},$$

for $1 < i < (n-1)$, $1 < j < n$.

Proof. As we can write $v(x, y)$ as a linear combination of monomials, i.e.

$$v(x, y) = \sum_{0 \leq i+j \leq 2} v'_{i,j} x^i y^j,$$

we need to show that each $x^i y^j$ can be written as a linear combination of basis functions on $D_{\alpha,\beta}$. This can be done by checking the nodal values of a combination of nodal basis functions at the Lagrange nodes on $D_{i,j}$. To this purpose, we denote the values on the diamond shaped region $D_{i,j}$ by a matrix. For example, see Figure 13, the nodal values of $\tau_{i,j}$ on $D_{i,j}$ form this matrix,

$$L_{i,j,i,j} = 2 \begin{pmatrix} & & & & 1/2 \\ & & & & 3/4 & 7/8 & 3/4 \\ & & & & 1/2 & 7/8 & 1 & 7/8 & 1/2 \\ & & & & & 3/4 & 7/8 & 3/4 \\ & & & & & & & & 1/2 \end{pmatrix},$$

where the first index set (i, j) comes from the basis function $\tau_{i,j}$, and the second index set (i, j) comes from the region $D_{i,j}$. As we consider the values on $D_{i,j}$ only, we drop the second set of index above, i.e.,

$$L_{k,l} = L_{k,l,i,j}.$$

We are left to compute summations of matrices. For example,

$$\begin{pmatrix} & & & & 1 \\ & & & & 1 & 1 & 1 \\ 1 & 1 & 1 & 1 & 1 \\ & & & & 1 & 1 & 1 \\ & & & & & & & & 1 \end{pmatrix} = \frac{1}{2} (L_{i-2,j} + L_{i,j-2} + L_{i,j} + L_{i+2,j} L_{i,j+2}).$$

The matrix on the left in above equation stands for the nodal values of constant function 1. In the same fashion, we found (the combinations are not unique)

$$\begin{aligned}
1 &= \frac{1}{2}(L_{i-2,j} + L_{i,j-2} + L_{i,j} + L_{i+2,j}L_{i,j+2}), \\
1 - \hat{x} &= \frac{1}{4}(2L_{i,j+2} + 2L_{i+2,j} + L_{i,j} + L_{i+1,j+1} - L_{i-1,j-1}), \\
\hat{y} &= \frac{1}{4}(2L_{i-2,j} + 2L_{i,j+2} + L_{i+1,j+1} + L_{i,j} - L_{i+1,j-1}), \\
(1 - \hat{x})^2 &= \frac{1}{2}(L_{i,j+2} + L_{i+1,j+1} + L_{i+2,j}), \\
\hat{y}^2 &= \frac{1}{2}(L_{i-2,j} + L_{i-1,j+1} + L_{i,j+2}), \\
\hat{x}\hat{y} &= \frac{1}{4}(3L_{i-2,j} + L_{i,j} + L_{i+2,j} - L_{i+1,j+1} - L_{i+1,j-1}).
\end{aligned}$$

Here we used the notations $\hat{x} = (x - x_i)/(h/2)$ and $\hat{y} = (y - y_i)/(h/2)$. Combining 1, $(1 - \hat{x})$ and $(1 - \hat{x})^2$ again, we would get \hat{x} and \hat{x}^2 . Thus

$$v(x, y) = \sum_{0 \leq i+j \leq 2} v'_{i,j} x^i y^j = \sum_{(k,l) \in M} v_{k,l} \tau_{i+k,j+l}(x, y).$$

■

Remark 4.1 *It is difficult to verify the proof of Lemma 4.1, i.e., the equalities there, without a computer. We give a different proof below. It would also help us to understand more the structure of nodal basis functions $\tau_{i,j}$. In Figure 15, we print the coefficients of $\tau_{i,j}$ on its 9 diamonds of support. There, we shift the center of each diamond for $D_{k,l}$ to the origin. Otherwise, we need to do a shifting and a scaling, for example,*

$$p_1 = 2 - x^2 - y^2 \longrightarrow p_1 = 2 - \frac{4(x - x_i)^2}{h^2} - \frac{4(y - y_j)^2}{h^2}. \quad (4.2)$$

By Figure 15, it is easy to see that

$$\begin{aligned}
\hat{x}^2 &= \tau_{i,j-2} + \tau_{i,j+2}, \\
\hat{y}^2 &= \tau_{i-2,j} + \tau_{i+2,j}, \\
2 - \hat{x}^2 - \hat{y}^2 &= \tau_{i,j}, \\
1 - 2\hat{x}^2\hat{y}^2 &= \tau_{i-1,j+1} + \tau_{i+1,j-1}, \\
2\hat{x} &= \tau_{i,j-2} + \tau_{i-1,j-1} - \tau_{i,j+2} - \tau_{i-1,j+1}, \\
2\hat{y} &= \tau_{i-2,j} + \tau_{i-1,j-1} - \tau_{i+2,j} - \tau_{i+1,j-1},
\end{aligned}$$

where $\hat{x} = (x - x_i)/(h/2)$ and $\hat{y} = (y - y_i)/(h/2)$. Making a few additional linear combinations, we would get 1, \hat{x} , \hat{y} , \hat{x}^2 , $\hat{x}\hat{y}$ and \hat{y}^2 be represented by linear combinations of nodal basis functions, on $D_{i,j}$. Therefore, this provides another way to prove Lemma 4.1.

We construct an averaging interpolation operator, cf. [22, 26], in order to prove the approximation property of the linear finite element vector space. This is done by finding a dual basis of 9 $\tau_{k,l}$ supported on 9 diamonds, see Figure 14,

$$B_{i,j} = \cup_{(k,l) \in M, \text{ defined in (4.1)}} D_{i+k,j+l}.$$

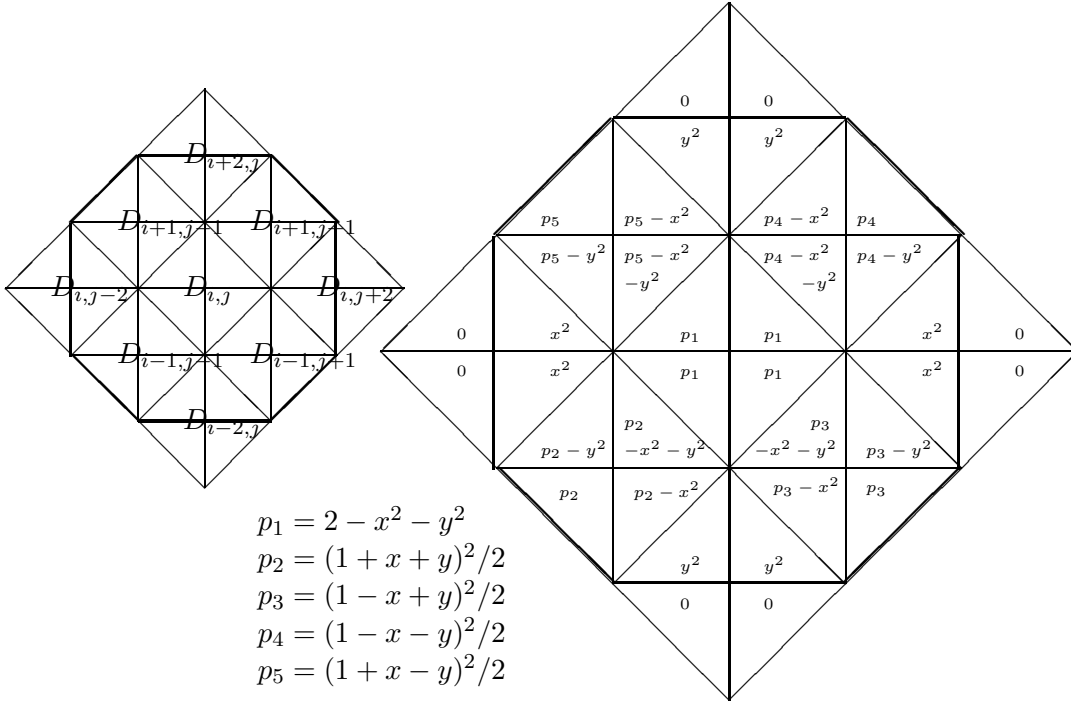


Figure 15: Definition of $\tau_{i,j}$, cf. (4.2).

There is a unique

$$\gamma_{i,j}(x, y) = \begin{cases} \sum_{(k,l) \in M} b_{k,l} \tau_{i+k,j+l}(x, y), & (x, y) \in B_{i,j}, \\ 0 & \text{elsewhere,} \end{cases} \quad (4.3)$$

such that

$$\int_{B_{i,j}} \tau_{i+k,j+l}(x, y) \gamma_{i,j}(x, y) d\mathbf{x} = \begin{cases} 1, & (k, l) = (0, 0), \\ 0, & \text{rest } (k, l) \in M. \end{cases} \quad (4.4)$$

For completeness, we give an explicit construction of the dual basis $\gamma_{i,j}$.

Let matrix $A = (a_{l,m})_{9 \times 9}$ represent the $L^2(B_{i,j})$ -inner products of 9 functions $\tau_{i',j'}$ which are supported in part on $B_{i,j}$, i.e.,

$$a_{M_l, m, M_{l'}, m'} = \int_{B_{i,j}} \tau_{i+l, j+m}(x, y) \tau_{i+l', j+m'}(x, y) dy dx,$$

where $M_{l,m}$ is an index, from 1 to 9, for the set M defined in (4.1):

$$\begin{aligned}
M_{-2,0} &= 1, & M_{-1,-1} &= 2, & M_{-1,1} &= 3, & M_{0,-2} &= 4, & M_{0,0} &= 5, \\
M_{0,2} &= 6, & M_{1,-1} &= 7, & M_{1,1} &= 8, & M_{2,0} &= 9, & & &
\end{aligned} \quad (4.5)$$

and $a_{l,m}$ is the l -th row m -th column element of the matrix. $n - th$ component of vector $\gamma^{(k)}$. By (3.4), we calculate the matrix

$$A = \frac{h^2}{180} \begin{pmatrix} 1336 & 654 & 654 & 35 & 264 & 35 & 6 & 6 & 0 \\ 654 & 1502 & 264 & 654 & 708 & 6 & 264 & 36 & 6 \\ 654 & 264 & 1502 & 6 & 708 & 654 & 36 & 264 & 6 \\ 35 & 654 & 6 & 1336 & 264 & 0 & 654 & 6 & 35 \\ 264 & 708 & 708 & 264 & 1680 & 264 & 708 & 708 & 264 \\ 35 & 6 & 654 & 0 & 264 & 1336 & 6 & 654 & 35 \\ 6 & 264 & 36 & 654 & 708 & 6 & 1502 & 264 & 654 \\ 6 & 36 & 264 & 6 & 708 & 654 & 264 & 1502 & 654 \\ 0 & 6 & 6 & 35 & 264 & 35 & 654 & 654 & 1336 \end{pmatrix}.$$

We invert the matrix A , which also shows that the functions $\{\tau_{i,j}\}$ are linearly independent on any finite domain larger than $B_{i,j}$. We note again that the set $\{\tau_{i,j}\}$ on the whole plane R^2 is not linearly independent, as pointed out by Chui and Wang [6, 7]. This can be seen in the proof of Lemma 4.1 where we have 9 degrees of freedom to match a 6 d.o.f. P_2 polynomial on each triangle. Such a non-uniqueness in combination is chain-likely to infinity. However, the boundary conditions defining the finite element spaces would eliminate extra $\tau_{i,j}$ functions at the boundary. Let $B = A^{-1}$. By the 5-th column numbers of B , we obtain the coefficients $b_{k,l}$ of the dual basis function $\gamma_{i,j}(x, y)$ in (4.3).

$$\begin{aligned} \gamma_{i,j} = \frac{h^{-2}}{4429496} & (583704\tau_{i-2,j} - 970452\tau_{i-1,j-1} - 970452\tau_{i-1,j+1} \\ & + 583704\tau_{i,j-2} + 1743594\tau_{i,j} + 583704\tau_{i,j+2} \\ & - 970452\tau_{i+1,j-1} - 970452\tau_{i+1,j+1} + 583704\tau_{i+2,j}). \end{aligned} \quad (4.6)$$

We introduce the following notations in order to express $\gamma_{i,j}$ triangle wise. Let $T_{i,j,k}$ be the four triangles forming the diamond $D_{i,j}$, see Figure 14. Then $\gamma_{i,j}(x, y)$ will be defined via the following 4 functions.

$$\begin{aligned} \gamma^{(1)} = & \begin{pmatrix} 196956 - 583704x^2 - 1554156y^2 - 1940904y \\ -485403 + 1743594y + 1842249y^2 + 1743594x + 1842249x^2 + 576186xy \\ -485403 + 1743594y + 1842249y^2 - 1743594x - 871797x^2 - 576186xy \\ 196956 - 1940904x - 1554156x^2 - 583704y^2 \\ 1546284 - 1159890y^2 - 1159890x^2 \\ 196956 + 1940904x + 2130342x^2 - 583704y^2 \\ -485403 - 1743594y - 871797y^2 + 1743594x + 1842249x^2 - 576186xy \\ -485403 - 1743594y - 871797y^2 - 1743594x - 871797x^2 + 576186xy \\ 196956 + 2130342y^2 + 1940904y - 583704x^2 \end{pmatrix}, \\ \gamma^{(2)} = & \begin{pmatrix} 196956 - 583704x^2 - 1554156y^2 - 1940904y \\ -485403 + 1743594y + 1842249y^2 + 1743594x - 871797x^2 + 576186xy \\ -485403 + 1743594y + 1842249y^2 - 1743594x + 1842249x^2 - 576186xy \\ 196956 - 1940904x + 2130342x^2 - 583704y^2 \\ 1546284 - 1159890y^2 - 1159890x^2 \\ 196956 + 1940904x - 1554156x^2 - 583704y^2 \\ -485403 - 1743594y - 871797y^2 + 1743594x - 871797x^2 - 576186xy \\ -485403 - 1743594y - 871797y^2 - 1743594x + 1842249x^2 + 576186xy \\ 196956 + 2130342y^2 + 1940904y - 583704x^2 \end{pmatrix}, \end{aligned}$$

$$\gamma^{(3)} = \begin{pmatrix} 196956 - 583704x^2 + 2130342y^2 - 1940904y \\ -485403 + 1743594y - 871797y^2 + 1743594x + 1842249x^2 + 576186xy \\ -485403 + 1743594y - 871797y^2 - 1743594x - 871797x^2 - 576186xy \\ 196956 - 1940904x - 1554156x^2 - 583704y^2 \\ 1546284 - 1159890y^2 - 1159890x^2 \\ 196956 + 1940904x + 2130342x^2 - 583704y^2 \\ -485403 - 1743594y + 1842249y^2 + 1743594x + 1842249x^2 - 576186xy \\ -485403 - 1743594y + 1842249y^2 - 1743594x - 871797x^2 + 576186xy \\ 196956 + 1940904y - 583704x^2 - 1554156y^2 \end{pmatrix},$$

and

$$\gamma^{(4)} = \begin{pmatrix} 196956 - 583704x^2 + 2130342y^2 - 1940904y \\ -485403 + 1743594y - 871797y^2 + 1743594x - 871797x^2 + 576186xy \\ -485403 + 1743594y - 871797y^2 - 1743594x + 1842249x^2 - 576186xy \\ 196956 - 1940904x + 2130342x^2 - 583704y^2 \\ 1546284 - 1159890y^2 - 1159890x^2 \\ 196956 + 1940904x - 1554156x^2 - 583704y^2 \\ -485403 - 1743594y + 1842249y^2 + 1743594x - 871797x^2 - 576186xy \\ -485403 - 1743594y + 1842249y^2 - 1743594x + 1842249x^2 + 576186xy \\ 196956 + 1940904y - 583704x^2 - 1554156y^2 \end{pmatrix}.$$

The dual basis function $\gamma_{i,j}(x, y)$ in (4.3) and (4.6) can be expressed as

$$\gamma_{i,j}(x, y) = \begin{cases} \frac{h^{-2}}{4429496} \gamma_{M_{l,m}}^{(k)} \left(\frac{x-x_i}{h}, \frac{y-y_j}{h} \right), & (x, y) \in T_{i,j,k}, \\ 0, & \text{elsewhere,} \end{cases} \quad (4.7)$$

where $M_{l,m}$ is an index for the index set M , defined in (4.5) and (4.1) respectively, and $\gamma_n^{(k)}(x, y)$ is the n -th component of vector $\gamma^{(k)}$.

Lemma 4.2 *The set of functions*

$$\{\tau_{2i-1,2j}, \tau_{2j,2i-1}, 1 < i < (n-1), 1 < j < n\}$$

is linearly independent as vectors in $L^2(\Omega)$ and the set forms a basis for the finite element space W_h defined in (3.6).

Proof. Let $w_h \in W_h$ be such that

$$w_h = \sum_{i,j} v_{i,j}^{(1)} \tau_{i,j}(x, y) = \sum_{i,j} v_{i,j}^{(2)} \tau_{i,j}(x, y).$$

Then, by (4.4), we conclude the proof with

$$v_{k,l}^{(1)} = \int_{\Omega} w_h \gamma_{k,l} dx dy = \sum_{k,l} v_{i,j}^{(2)} \int_{\Omega} \tau_{i,j} \tau_{k,l} dx dy = v_{k,l}^{(2)}.$$

■

We are able to define an L^2 averaging interpolation operator next:

$$\begin{aligned}
I_h &: H_0^2(\Omega) \rightarrow W_h, \\
I_h &: w \mapsto I_h w = \sum_{i=2}^{n-2} \sum_{j=1}^{n-1} (w_{2i-1,2j} \tau_{2i-1,2j}(x, y) + w_{2j,2i-1} \tau_{2j,2i-1}(x, y)), \\
w_{i,j} &= \int_{B_{i,j}} \gamma_{i,j}(x, y) w(x, y) d\mathbf{x}.
\end{aligned}$$

By this definition and Lemma 4.1, it is standard to show the stability and the approximation property for the interpolation operator, cf. [22, 26],

$$\begin{aligned}
\|I_h w\|_{H^i(\Omega)} &\leq C \|w\|_{H^i(\Omega)}, \quad i = 0, 1, 2, \\
\|w - I_h w\|_{H^i(\Omega)} &\leq C h^{r-i} \|w\|_{H^r(\Omega)}, \quad i = 0, 1, 2, \quad 2 \leq r \leq \min\{i + 2, 3\}.
\end{aligned} \tag{4.8}$$

Theorem 4.1 *The finite element solutions of (3.7) converge to the exact solution of biharmonic equation (3.5) in the optimal order:*

$$|w - w_h|_{H^1} + h|w - w_h|_{H^2} \leq C h^2 |f|_{H^{-1}}. \tag{4.9}$$

Proof. The finite element solution is the orthogonal projection of w in W_h , in the semi- H^2 inner-product. By Cea's lemma (cf. [4]) and the optimal order approximation in (4.8), w_h converges in the optimal order:

$$|w - w_h|_{H^2} \leq C h |w|_{H^3}.$$

Then we apply the duality argument for the error in semi- H^1 norm. We obtain (4.9) by the elliptic regularity on convex domain Ω for the biharmonic equation, cf. [12]. \blacksquare

We are ready to study the approximation property of divergence-free finite elements. We relate the Stokes equations (2.1) to the following biharmonic equation: Find $w \in H_0^2(\Omega)$, such that

$$(\Delta w, \Delta s) = -(\operatorname{curl} \mathbf{f}, s) \quad \forall s \in H_0^2(\Omega). \tag{4.10}$$

It is well known [19] that

$$\operatorname{curl} H_0^2(\Omega) = \mathbf{Z} \quad \text{and} \quad \operatorname{curl} w = \mathbf{u}. \tag{4.11}$$

Here \mathbf{u} and \mathbf{f} are defined in (2.1). As the domain is convex, by [12], for any $g \in H^{-1}(\Omega)$, the unique weak solution $w \in H_0^2(\Omega)$ of the biharmonic equation (3.5) satisfies

$$\|w\|_{H^{r+2}(\Omega)} \leq C \|g\|_{H^{r-2}(\Omega)}, \quad r \geq 1. \tag{4.12}$$

Theorem 4.2 *Let the smooth solution w in (4.10) have the elliptic regularity (4.12). The unique solution \mathbf{u}_h of the discrete Stokes equations (2.7) approximate that of (2.1) in the optimal order:*

$$\|\mathbf{u} - \mathbf{u}_h\|_{H^2(\Omega)^2} \leq C h \|\mathbf{f}\|_{L^2(\Omega)^2}. \tag{4.13}$$

Proof. Let $w_h \in W_h$ be the finite element solution for the biharmonic problem (4.10), i.e.,

$$(\Delta w_h, \Delta s_h) = -(\mathbf{curl} \mathbf{f}, s_h) \quad \forall s_h \in W_h. \quad (4.14)$$

By (4.9) and (4.11), since \mathbf{u}_h is the orthogonal projection of \mathbf{u} in \mathbf{Z}_h and $\mathbf{curl} w_h \in \mathbf{Z}_h$, it follows that

$$\begin{aligned} |\mathbf{u} - \mathbf{u}_h|_{H^1(\Omega)^2} &= \inf_{\mathbf{z}_h \in \mathbf{Z}_h} |\mathbf{u} - \mathbf{z}_h|_{H^1(\Omega)^2} \leq |\mathbf{u} - \mathbf{curl} w_h|_{H^1(\Omega)^2} \\ &= |\mathbf{curl} w - \mathbf{curl} w_h|_{H^1(\Omega)^2} \leq |w - w_h|_{H^2(\Omega)} \end{aligned} \quad (4.15)$$

$$\leq Ch|w|_{H^3(\Omega)} \leq Ch\|g\|_{H^1(\Omega)} \leq Ch\|f\|_{L^2(\Omega)^2}. \quad (4.16)$$

The L_2 error of the velocity is bounded by the H_1 error, ensured by the Poincaré inequality. ■

5 Numerical tests

In this section, we report some results of numerical experiments on the C_1 - P_2 element and the P_1 divergence-free element on union jack grids, over the unit square domain $\Omega = (0, 1)^2$. The first four levels of triangulations of the domain are plotted in Figure 16. We note that, other than the first level, the grids are of union jack type. Here the grids are refined by the bisection multigrid refinement, i.e., connect the midpoint of longest edge in a triangle to the opposite vertex and to the two midpoints on the other two edges. By this multigrid refinement, a union jack grid would be refined into another nested union jack grid, shown in Figure 16.

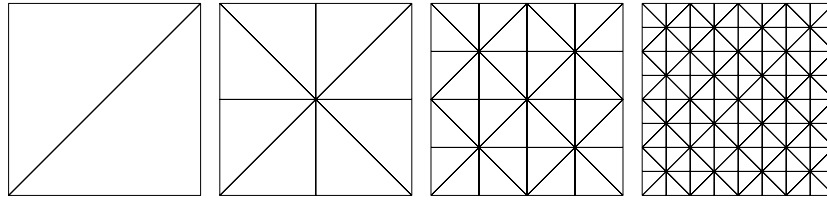


Figure 16: First 4 grids in computation, by the bisection multigrid refinement.

We first solve the biharmonic equation (3.5) where the exact solution is

$$w = 2^{10}(x - x^2)^2(y - y^2)^2.$$

The solution w is plotted in Figure 17.

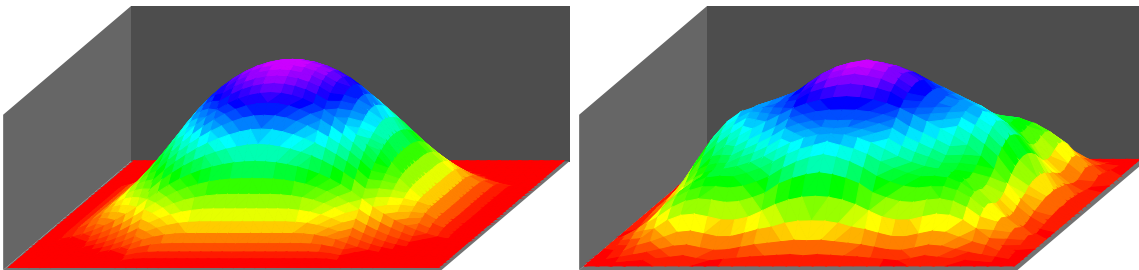


Figure 17: The exact solution and the error, for w , on level 4 grid.

We solve the C_1 - P_2 finite element equations (3.7) on several levels of grid. The error $w - w_h$ on the 4th level grid is plotted in Figure 17. All the errors in various measurements are listed in Table 1. We can see from the table that both the H^2 and the H^1 convergence of the C_1 - P_2 element are in optimal order, as guaranteed by Theorem 4.1. However, the L^2 and l^∞ errors seem to be in suboptimal orders, not order 3. We do not have any theory or explanation yet.

Table 1: C_1 - P_2 errors, $e_w = w - w_h$, for the biharmonic equation.

Level	$ e_w _{H^2}$	$O(h^r)$	$ e_w _{H^1}$	$O(h^r)$	$\ e_w\ _{L^2}$	$O(h^r)$	$ e_w _{l^\infty}$	$O(h^r)$
4	23.40055		2.12731		0.43421		0.93963	
5	12.18107	0.94	0.56678	1.90	0.11695	1.89	0.24137	1.96
6	6.14795	0.98	0.14405	1.97	0.02983	1.97	0.06083	1.98
7	3.08095	0.99	0.03616	1.99	0.00750	1.99	0.01524	1.99

Next, we test the P_1 divergence-free element for solving the Stokes equations (2.1), where we choose the exact solutions as

$$\mathbf{u} = \begin{pmatrix} g_y \\ -g_x \end{pmatrix}, \quad p = g_{xx}, \quad (5.1)$$

where

$$g = 2^6(x - x^2)^2(y - y^2)^2. \quad (5.2)$$

The first component of \mathbf{u} is plotted in Figure 18.

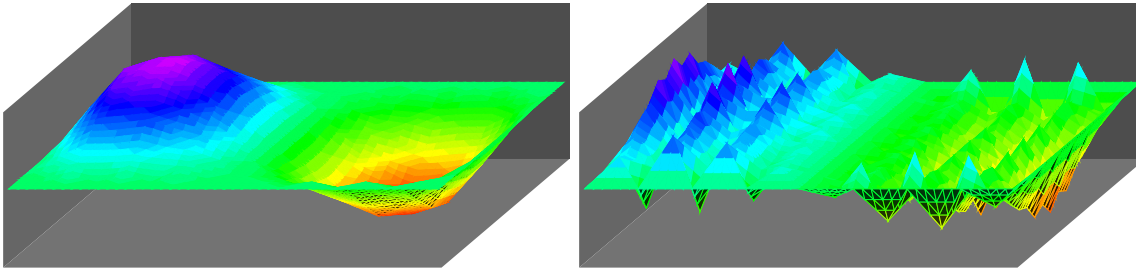


Figure 18: The exact solution and the error, of first component of \mathbf{u} on level 4 grid.

The grids for computation is shown in Figure 16. The error $\mathbf{u} - \mathbf{u}_h$ is shown in Figure 18, on the 4th level of grid. The errors in semi- H^1 norm are listed in Table 2. The H^1 convergence rate is optimal, as stated in Theorem 4.2. Here the l^∞ error (maximal nodal error) also converges at the optimal order, but not proved in this manuscript.

Next, we show a numerical example which indicates the approximation property of P_1 divergence-free elements would disappear without the special structure of underlying union jack grids. It is known as locking. We perturb the union jack grids as shown in Figure 19. The errors are listed in Table 3. As we can see from the results, the only divergence-free P_1 function on such grids would be 0 which has absolutely no approximation to the true solution.

The union jack grids are 45-degree rotations of uniform criss-cross grids, cf. Figure 2. However, the stability of P_1 - P_0 on the two types of grids are different. In [18], it is shown that the stability of P_1 - P_0 elements on uniform criss-cross grids is related to that of Q_1 - Q_0 elements on uniform squares, though the inf-sup condition fails for the element. Nevertheless,

Table 2: P_1 elements on union jack grids for the Stokes equations.

Level	$ \mathbf{u} - \mathbf{u}_h _{H^1}$	Order	$ \mathbf{u} - \mathbf{u}_h _{L^\infty}$	Order
4	2.42445		0.42187	
5	1.60380	0.59	0.25639	0.71
6	0.83528	0.94	0.06972	1.87
7	0.42161	0.98	0.01782	1.96

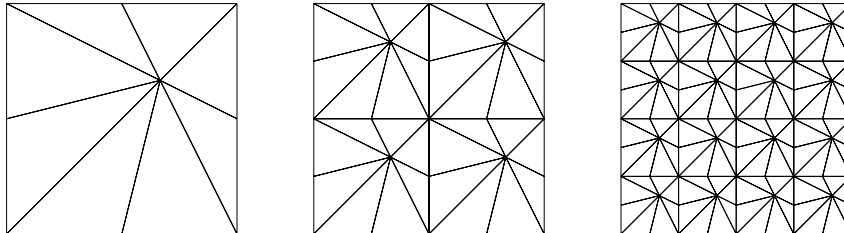


Figure 19: The perturbed union jack grids for the tests in Table 3.

the convergence holds for the element on criss-cross grid, but it fails on uniform union jack grids, as shown in the next numerical test. Here we compute the P_0 pressure solutions too, which converge on criss-cross grids, but does not on union jack grids, as shown in Table 4. Again, the criss-cross grid is a 45-degree rotation of a union jack grid. But one provides correct solutions for the pressure while the other fails completely. Further analysis is needed on the element on both types of grids.

In the next numerical computation, we solve a simple model problem of Stokes flow. By identifying the low strain region, we can further use special models in the low strain flow region, such as a non-Newtonian fluid model, or a two-phase flow model, or a viscoelastic fluid model, depending on the fluid, cf. [23]. We choose this model of computation to show a difference between the method of using the C_0 - P_1 divergence-free basis for \mathbf{u}_h by (2.15) or of computing a C_1 - P_2 stream function w of (4.11) and the method of solving the mixed element system (2.7) directly. It is very difficult to use (2.15) or (4.11) when the boundary condition is inhomogeneous. However, for the mixed element method (2.7), we simply interpolate $\mathbf{u}|_{\partial\Omega}$ by a $H^1(\Omega)$ function which vanishes in all internal nodes, to get $\mathbf{u}_{h,b}$ which is not divergence free. So we solve a linear system of equations (2.7) to get a $\mathbf{u}_{h,i} \in H_0^1$ so that $\mathbf{u}_h = \mathbf{u}_{h,b} + \mathbf{u}_{h,i}$ is divergence free, approximating the velocity \mathbf{u} . As shown in [27] that (2.7) always has a unique solution for all divergence-free elements. We use the iterated penalty method to solve (2.7),

Table 3: P_1 elements fail to converge on perturbed union jack grids.

Level	$ \mathbf{u} - \mathbf{u}_h _{L^\infty}$	Order	$ \mathbf{u} - \mathbf{u}_h _{H^1}$	Order
3	0.75000		3.20715	
4	0.74593	—	3.52043	—
5	0.73562	—	3.49121	—
6	0.74417	—	3.54536	—

Table 4: Convergence for the P_1 - P_0 element on union jack grids and criss-cross grids.

Level	$ \mathbf{e}_u _{L^\infty}$ order	$ \mathbf{e}_u _{H^1}$ order	$ e_p _{L^\infty}$ order	$\ e_p\ _{L^2}$ order
On uniform union jack grids, cf. Figure 2(C)				
3	0.42187	2.4244	9.547	5.659
4	0.25639 0.71	1.6038 0.59	10.263 —	6.914 —
5	0.06972 1.88	0.8352 0.94	10.157 —	6.618 —
6	0.01782 1.97	0.4216 0.99	10.159 —	6.499 —
On uniform criss-cross grids, cf. Figure 2(B)				
3	0.21399	1.3679	2.717	2.041
4	0.07262 1.55	0.6976 0.97	1.738 0.64	1.036 0.98
5	0.02063 1.81	0.3491 1.00	0.966 0.84	0.519 1.00
6	0.00549 1.91	0.1745 1.00	0.498 0.95	0.260 1.00
7	0.00142 1.95	0.0872 1.00	0.253 0.98	0.130 1.00

cf. [4]. Though the linear system (2.7) is not stable and the discrete pressure solution does not approximate the true solution, \mathbf{u}_h does converge to \mathbf{u} in optimal order, as shown by our theory.

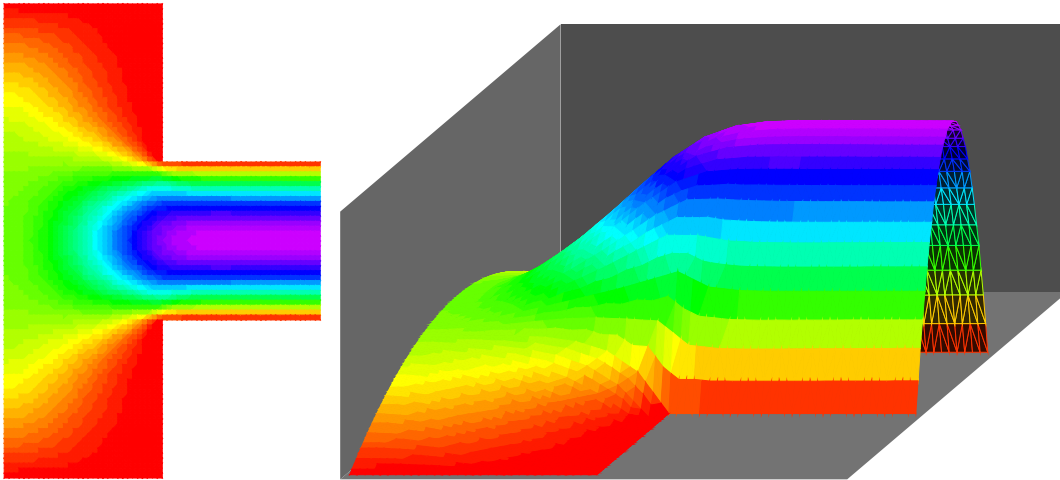


Figure 20: The first component of a computed velocity field.

As shown in Figure 4, we have inhomogeneous boundary conditions where the in-flow BC is $\langle y(3-y), 0 \rangle$ and the out-flow BC $\langle 27(y-1)(2-y), 0 \rangle$. One coarse grid in computation is shown in the first graph in Figure 4. The second graph is a computed velocity field, showing the flow direction and speed. We show the first component of computed \mathbf{u}_h , $\mathbf{u}_{h,1}$ in Figure 20. The third graph is the computed modulus of the strain tensor:

$$|E| = (2(\mathbf{u}_{1,x}^2 + \mathbf{u}_{2,y}^2) + (\mathbf{u}_{1,y} + \mathbf{u}_{2,x})^2)^{1/2}.$$

We draw a rough region where $|E| \leq \epsilon$ and further modeling would be applied.

Finally, we show by the last numerical test that the P_1 divergence-free element space may keep its approximation power when the perturbed union jack grids consist only rectangles

or parallelograms everywhere except at the boundary. In the test, we chose a parallelogram domain, with four vertices $(0, 0)$, $(1, 0)$, $(3/2, 1)$ and $(1/2, 1)$, for the Stokes equation 2.1, where the right hand function is determined by (5.1) with a new function g ,

$$g(x, y) = 2^6(2x - y)^2(2 - 2x - y)^2(y - y^2)^2.$$

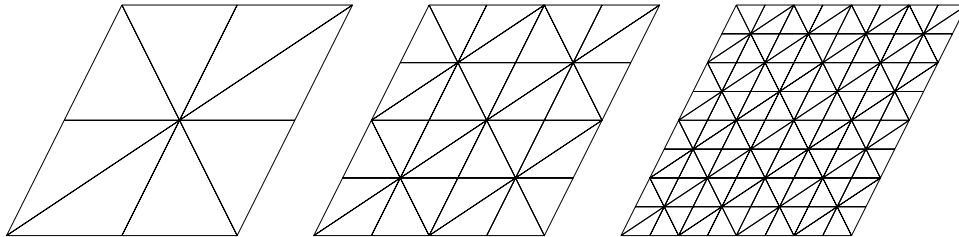


Figure 21: The uniform union grids on a parallelogram domain.

The grids are shown in Figure 21. The errors are listed in Table 5. The optimal order of convergence is shown in the table.

Table 5: P_1 elements on parallelogram union jack grids..

Level	$ \mathbf{u} - \mathbf{u}_h _{l^\infty}$	Order	$ \mathbf{u} - \mathbf{u}_h _{H^1}$	Order
3	12.00000		56.04713	
4	4.50835	1.41	28.67645	0.97
5	1.34418	1.74	14.89010	0.95
6	0.36909	1.86	7.50887	0.99
7	0.09435	1.96	3.72868	1.00

Acknowledgments. This work was done in June 2008 during the author’s visit to Dr. Xuejun Xu, sponsored by the Senior Researcher Visiting Program, at the State Key Laboratory of Scientific and Engineering Computing, Beijing, China.

References

- [1] D. N. Arnold, F. Brezzi, B. Cockburn and D. Marini, *Unified analysis of discontinuous Galerkin methods for elliptic problems*, SIAM J. Numer. Anal. 39 (2001/02), no. 5, 1749–1779.
- [2] D. N. Arnold and J. Qin, *Quadratic velocity/linear pressure Stokes elements*, in *Advances in Computer Methods for Partial Differential Equations VII*, ed. R. Vichnevetsky and R.S. Steplemen, 1992.
- [3] G. Awasou and M.-J. Lai, *Trivariate spline approximations of 3D Navier-Stokes equations*, Math. Comp. 74 (2004), 585–601.

- [4] S.C. Brenner and L.R. Scott, *The Mathematical Theory of Finite Element Methods*, Springer-Verlag, New York, 1994.
- [5] F. Brezzi and M. Fortin, *Mixed and hybrid finite element methods*, Springer, 1991.
- [6] C.K. Chui and R.-H. Wang, *Multivariate spline spaces*, J. Math. Anal. Appl. 94 (1983), 197–221.
- [7] C.K. Chui and R.-H. Wang, *On a bivariate B-spline basis*, Sci. Sinica XXVII (1984), 1129–1142.
- [8] B. Cockburn, F. Li and C.-W. Shu, *Locally divergence-free discontinuous Galerkin methods for the Maxwell equations*, J. Comput. Phys. 194 (2004), no. 2, 588–610.
- [9] C. Dagnino and P. Lamberti, *Numerical integration of 2-D integrals based on local bivariate quadratic C^1 quasi-interpolating splines*, Adv. Comput. Math.. 8 (1998), no. 1-2, 19-31.
- [10] C. Dagnino and P. Lamberti, *On the approximation power of bivariate quadratic C^1 splines*, J. Comput. Appl. Math. 131 (2001), no. 1-2, 321–332.
- [11] C. Dagnino and P. Lamberti, *Some performances of local bivariate quadratic C^1 quasi-interpolating splines on nonuniform type-2 triangulations*, J. Comput. Appl. Math. 173 (2005), no. 1, 21–37.
- [12] P. GRISVARD, *Elliptic Problems in Nonsmooth Domains*, Pitman Pub. Inc., 1985.
- [13] M.-J. Lai and P. Wenston, *Bivariate spline method for numerical solution of steady state NavierStokes equations over polygons in stream function formulation*, Numer. Methods PDE 19 (2003), 776–827.
- [14] M.-J. Lai and P. Wenston, *Bivariate splines for fluid flows*, Computers and Fluids 33 (2004), 1047–1073.
- [15] K. A. Mardal, X.-C. Tai and R. Winther, *A robust finite element method for Darcy-Stokes flow*, SIAM J. Numer. Anal. 40 (2002), 1605–1631..
- [16] J. Morgan and R. Scott, *A nodal basis for C^1 piecewise polynomials of degree $n \geq 5$* , 29, No. 131 (1975), 736–740.
- [17] M.J.D. Powell and M.A. Sabin, *Piecewise quadratic approximations on triangles*, ACM Transactions on Mathematical Software, 3-4 (1977), 316-325.
- [18] J. Qin and S. Zhang, *Stability and approximability of the P1-P0 element for Stokes equations*, Int. J. Numer. Meth. Fluids, 54 (2007), 497–515.
- [19] P. A. Raviart and V. Girault, *Finite element methods for Navier-Stokes equations*, Springer, 1986.
- [20] L. R. Scott and M. Vogelius, *Norm estimates for a maximal right inverse of the divergence operator in spaces of piecewise polynomials*, RAIRO, Modelisation Math. Anal. Numer. 19 (1985), 111–143.

- [21] L. R. Scott and M. Vogelius, *Conforming finite element methods for incompressible and nearly incompressible continua*, in Lectures in Applied Mathematics 22, 1985, 221–244.
- [22] L. R. Scott and S. Zhang, *Finite element interpolation of nonsmooth functions satisfying boundary conditions*, Math. Comp. 54 (1990), 483–493. e
- [23] D. N. Smyrniaios and J. A. Tsampoulos, *Squeeze flow of Bingham plastics*, J. Non-Newtonian Fluid Mech. 100 (2001), 165-190.
- [24] T. Sorokina and F. Zeilfelder, *Optimal quasi-interpolation by quadratic C^1 -splines on type-2 triangulations*, in Approximation theory XI: Gatlinburg 2004, 423–438, Mod. Methods Math., Nashboro Press, Brentwood, TN, 2005.
- [25] S. Zhang, *A new family of stable mixed finite elements for 3D Stokes equations*, Math. Comp. 74 (2005), 543–554.
- [26] S. Zhang, *A $C1$ - $P2$ finite element without nodal basis*, M2AN 42 (2008), 175-192.
- [27] S. Zhang, *On the $P1$ Powell-Sabin divergence-free finite element for the Stokes equations*, J. Comp. Math., 26 (2008), 456-470.
- [28] S. Zhang, *A family of 3D continuously differentiable finite elements on tetrahedral grids*, Applied Numerical Mathematics, 59, no. 1 (2009), 219–233.
- [29] P. B. Zwart, *Multivariate splines with non-degenerate partitions*, SIAM J. Numer. Anal. 10 (1973), 665-673.